



CrossMark
click for updates

Cite this: *RSC Adv.*, 2015, 5, 40236

Optically-transparent and electrically-conductive AgI–AgPO₃–WO₃ glass fibers†

Maxime Rioux,^{*ab} Yannick Ledemi,^b Jeff Viens,^b Steeve Morency,^b
Seyed Alireza Ghaffari^b and Younès Messaddeq^b

In this study, we report to our knowledge the first optically-transparent and electrically-conductive optical glass fiber belonging to the system AgI–AgPO₃–WO₃. The addition of tungsten oxide (WO₃) into the phosphate glassy network allowed the adjustment of the glass transition temperature, thermal expansion coefficient, refractive index, optical band edge, and electrical conductivity, which are all very important parameters in view of drawing glass fibers with a desired set of electrical and optical properties. Furthermore, the addition of WO₃ can improve considerably glass stability against water and humidity in the environment. AgI–AgPO₃–WO₃ glass fibers with 15 mol% WO₃ showed 2 dB m⁻¹ optical propagation loss from 800 to 950 nm wavelength range, and 10⁻³ S cm⁻¹ electrical conductivity at 1 MHz AC frequency. Complex impedance spectra and thermal activation energies ranging from 0.15 to 0.30 eV are indicative of a dominant conductivity mechanism being ionic in nature within the range of AC frequencies from 1 Hz to 1 MHz. Fibers exhibited higher electrical conductivities than the bulk glasses. Glasses in the AgI–AgPO₃–WO₃ system can be used for fibers that require a set of adjustable properties pertaining to electrical conductivity, optical transparency, and environmental stability.

Received 14th January 2015

Accepted 20th April 2015

DOI: 10.1039/c5ra00681c

www.rsc.org/advances

1. Introduction

The development of multi-material optical fibers that transmit both light and electrical current represents one of many challenges in the field of multifunctional fibers.^{1–3} Phosphate-based glasses, depending on the glass composition, exhibit high solubility to metallic ions, high chemical and mechanical stability, and high glass transition and crystallization temperatures.^{4–7} In particular, the well-studied phosphate glasses belonging to the $x\text{AgI}-(1-x)\text{AgPO}_3$ pseudo-binary system provide high ionic AC conductivities at room temperature (*i.e.* $10^{-2} \geq \sigma \geq 10^{-3}$ S cm⁻¹). This set of attributes are of great interest to science and technology, as these glasses may form the basis for electro-optics modulator for telecommunication applications where an electrical field applied to the solid can modulate the phase, the frequency, the amplitude, or the polarization of the incident light passing through the material.^{8,9} They may also be used as microprobes to measure the electrical activity of nervous cells of the brain,¹⁰ or into smart textiles where electrically conductive fibers can be integrated inside yarns for different uses in biomedicine.^{11,12}

In recent years, extensive research has been conducted in the field of ion conductive glasses based on metal halides owing to their fast ion conduction properties.^{13–16} The best known metal halide superionic conductive crystalline compounds are rubidium silver iodide (RbAg₄I₅) and silver iodide (AgI). The latter is used extensively for ion-conductive glasses because of its low cost and high conductivity compared to RbAg₄I₅. The alpha phase of crystalline AgI ($\alpha\text{-AgI}$) is stable above 147 °C and can reach very high electrical conductivity (1 S cm⁻¹) owing to its body-centered cubic structure (bcc), with the four iodide ions (I⁻) in the unit cell in closed-packed positions with a space group $Im\bar{3}m$. The silver ions (Ag⁺) may be in either the octahedral sites, the tetrahedral sites, or between two adjacent iodide ions. It has been demonstrated that this crystalline structure includes 42 sites that provides mobility to the silver ions.^{17,18} Moreover, the coordination around the ions is weak which enables the silver ions to move from one site to another at very weak activation energies. The I⁻ anions are also highly polarizable, which enables the silver ions to move easily near the anions by the deformation of the electronic cloud. Below 147 °C, silver iodide AgI is in the β -phase which presents a closed wurtzite structure whereas its electrical conductivity decreases considerably to values ranging from 10⁻⁵ to 10⁻⁶ S cm⁻¹. Because of these remarkable electrical properties, many researches have been carried out to stabilize the α -phase at room temperature, including the exploration of different M_xO_y glassy matrices (*i.e.* B₂O₃, MoO₃, GeO₂, WO₃)^{19–22} and polymer-coated AgI nanoparticles.²³ In M_xO_y glassy matrices, the

^aDepartment of Chemistry, Laval University, Quebec, Canada. E-mail: maxime.rioux.2@ulaval.ca

^bCentre d'Optique, Photonique et Laser, Université Laval, 2375 rue la Terrasse, local 2131, Québec (Qc), G1V 0A6, Canada

† Electronic supplementary information (ESI) available. See DOI: 10.1039/c5ra00681c

α -phase has been stabilized by cooling the glass liquid very rapidly into flake-like samples by using fast roller-quenching methods used for the fabrication of metallic glasses. The cooling was so rapid that the transition between the α -phase and the β -phase did not occur. Unfortunately, it is impractical to use such as-prepared glasses due to their high mechanical fragility related to the stress induced during fast quenching. However, AgI can still be incorporated in many glassy matrices at relatively high concentrations to produce low-to-medium ion conductive glasses such as the AgI-Ag₂O-M_xO_y and AgI-AgPO₃-MO_x systems.^{24–27} The reported highest conductivities for these glasses are in the range 10⁻³ to 10⁻² S cm⁻¹ at room temperature.

Different mechanisms have been proposed over the last thirty years to explain the ionic conductivity in AgI-containing glasses, especially in AgI-AgPO₃ glasses: the diffusion path model,²⁸ the cluster model,^{29–31} the cluster tissue model^{32,33} or the weak electrolyte model.^{34–36} In all these models, the conduction process depends on the presence of Ag⁺ ions, and the magnitude of ionic conductivity depends on the charge carrier concentration. In the 90's, a Monte Carlo model³⁷ was proposed to explain neutron and X-ray diffraction results on AgI-AgPO₃ glasses of different compositions. It was also proposed that the presence of iodide in AgI decreases the activation energy required for the Ag ions to move from one vacant site to another, thus improving carrier mobility and electrical conductivity in AgI-AgPO₃ glasses, as experimentally evidenced.³⁸

In the present work, we have investigated a new glass composition belonging to the AgI-AgPO₃-WO₃ pseudo-ternary system. Vitreous AgPO₃ silver phosphate was selected as the main glass former owing to the high metal ions solubility characteristic to phosphate glassy network. Tungsten trioxide WO₃ was added to increase the glass mechanical and chemical stability, particularly its stability against water degradation. We report on the fabrication and characterization of electrically-conductive bulk glasses, including electrical conductivity measurements at room temperature. Finally, glass preforms of determined composition were produced and successfully drawn into fibers with good electrical conduction and light

transmission properties. To the best of our knowledge, this is the first report of light and electrical conduction in AgI-AgPO₃-WO₃ glass optical fiber.

2. Experimental

2.1 Bulk glass synthesis and optical fiber fabrication

Materials. Tungsten(vi) oxide powder (99.9%) and ammonium phosphate monobasic ($\geq 98.5\%$, *ReagentPlus*®) were both obtained from Sigma Aldrich. Silver iodide (99.9%) and silver nitrate (99.9%, ACS grade) were both obtained from Alfa Aesar. All reagents were used as received.

Synthesis procedure. As a first step, the silver metaphosphate (AgPO₃) matrix has been synthesized using a mixture of silver nitrate (AgNO₃) and ammonium phosphate monobasic (NH₄H₂PO₄) in a mass ratio AgNO₃/NH₄H₂PO₄ of 1.48. First, the mixture was loaded in an alumina crucible and heated at 100 °C during 20 h to allow the evaporation of residual water. The mixture was then heated to 350 °C at a rate of 2 °C min⁻¹ and kept at this temperature during 24 h to allow the two compounds to react completely together to form AgPO₃. The AgPO₃ was then heated to 500 °C and kept at that temperature during 60 minutes to decrease its viscosity and facilitate its casting into a stainless steel mold at room temperature. The resulting glass was grinded into a fine powder for further use. In a second step, the AgI-AgPO₃-WO₃ glasses were prepared from high purity AgI, WO₃, and the as-prepared AgPO₃. The three compounds were mixed together with the desired molar ratio and loaded in a fused silica crucible according to the following composition law: 45AgI-(55 - x)AgPO₃-xWO₃ with x = 0, 5, 10, 15, 20 and 25 mol%. The mixture was then placed in a resistive furnace at a temperature of 1000 °C. After 5 minutes, the melt was manually agitated to assure its good homogeneity. After another 5 minutes, the glass melt was cooled in a 10 mm diameter cylindrical brass mold preheated at the glass transition temperature (*T_g*). The glass was then placed into a resistive oven at the annealing temperature for 5 h and subsequently cooled down to room temperature in approximately 10 hours to remove any residual stress induced during the quenching. Finally, the glass sample was polished using silicon carbide

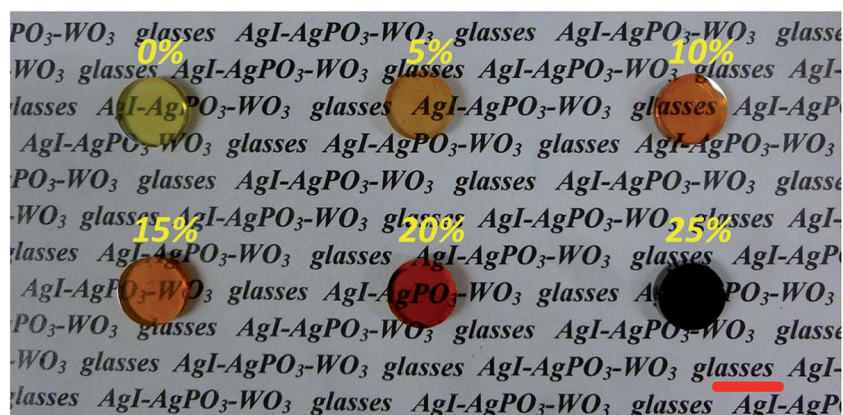


Fig. 1 Photograph of 45AgI-(55 - x)AgPO₃-xWO₃ glasses with x varying from 0 to 25 mol% (scaling bar: 10 mm).

(SiC) polishing papers with decreasing grit size (400, 600, 800) before using a 1/8 micron diamond colloid mixed with ethanol to obtain sufficient surface quality for optical characterization (Fig. 1).

To fabricate optical fibers, cylindrical glass preforms of 70 mm of length and 10 mm of diameter were prepared according to the abovementioned procedure. The surface of the glass preforms were then polished to obtain a smooth surface prior to fiber drawing. This polishing step prevented the growth of defects at the preform surface during fiber drawing, which otherwise resulted in poor mechanical resistance or even breakage of the glass fiber. The glass preforms were drawn into fibers with controlled diameters of 125 and 250 μm in a 7 meter optical fiber drawing tower set at a temperature of 300 $^{\circ}\text{C}$, giving 60 and 20 m long fibers for the 125 and 250 μm diameters, respectively. During the fiber fabrication process, a UV-cured polymer coating (DeSolute® DS-2015) was applied to the fiber surface to improve its mechanical resistance. All the glass fabrication steps and the characterizations have been performed under ambient atmosphere at a temperature of 20 $^{\circ}\text{C}$ and relative humidity of 40%.

2.2 Material characterizations

Elemental analysis and thermal characterization. The stoichiometry of the glasses has been determined using a CAMECA-SX100 (Cameca, Gennevilliers, France) electron probe micro-analyzer to demonstrate the reproducibility of the method used for the glass fabrication. The analysis was performed by wavelength-dispersive spectroscopy (WDS) using an electron microprobe (EPMA) with an accelerating voltage of 15 kV and a current of 20 nA. Each glass composition has been analyzed on three different samples with eight quantitative measurements on each.

Differential scanning calorimetric (DSC) measurements were performed using a Netzsch DSC Pegasus 404F3 apparatus on small glass pieces into sealed Al pans at a heating rate of 10 $^{\circ}\text{C min}^{-1}$ up to a temperature of 600 $^{\circ}\text{C}$. The thermal expansion coefficient (TEC) measurements were measured using a Netzsch TMA hyperion 402F1 apparatus on glass rods of 5 mm length at a heating rate of 5 $^{\circ}\text{C min}^{-1}$ up to 100 $^{\circ}\text{C}$ and a load of 0.02 N. The TEC was determined in the temperature range from 20 to 100 $^{\circ}\text{C}$.

Optical and electrical characterizations. The optical transmission spectra were measured by using a UV-VIS-NIR Varian Cary 500 double beam spectrophotometer on polished 3 mm-thick samples. Linear refractive index has been measured by using the prism coupling technique (M-lines Metricon 2010) at 633, 972, 1308 and 1538 nm with a precision of ± 0.001 . To measure the optical fiber propagation loss, we used a fiber cut-back experimental set up comprising a SuperK COMPACT supercontinuum white light laser from NKT photonics, a monochromator from Brucker, and a 20 \times microscope objective from Olympus.

The electrical characterizations of the bulk glasses were performed using a 1260 Solartron impedance analyzer in the frequency range of 1 Hz to 1 MHz, with an applied voltage of 100 mV and zero bias with an accuracy of 0.1%. The 5 mm

thickness glass samples were disposed between two platinum electrodes Probostat TM (Norecs) probe sample holder embedded in a vertical resistive split furnace (Mellen) for temperature dependent measurements. The 2-point conductivity method with two outer platinum “hand” electrode contacts was used with a 4-terminal measuring device that eliminated lead or parasite resistances on the electrodes. To allow better contact between the platinum electrodes and the glass samples, silver paint was applied on both contact surfaces of the glasses.^{39,40} The silver paint used was colloidal silver from Pelco® with a sheet resistance of 0.02–0.05 ohms per square per mil and a service temperature range between -40 $^{\circ}\text{C}$ and 260 $^{\circ}\text{C}$. After application on the sample surface, the silver paint has been left overnight to dry at room temperature prior to further conductivity measurements. Electrical conductivity measurements were performed as a function of temperature, from room temperature up to a temperature close to the T_g for each sample. For the electrical conductivity characterization of the fibers, we used the Solartron impedance analyzer with a standard fiber holder.

Density and XPS measurements. The glass samples density was measured according to the Archimedes' principle by using a Mirage Alfa-MS densimeter with a measurement precision of ± 0.002 g cm^{-3} .

For the XPS analyses, an Axis-Ultra system Kratos (UK) spectrometer equipped with an electrostatic analyzer, an 8-channels detection system, a dual Al-Mg X-ray source without monochromator, and Al source at a power of 300 watts with a monochromator was used. The system also included an electron gun of very low energy for neutralizing the electrostatic charges that appeared on the electrically insulating samples upon exposure to monochromatic X-ray beam. This spectrometer was installed in a vacuum system with a base pressure of 7×10^{-8} Pa.

3. Results and discussion

3.1 Glass formation

In Fig. 1, we can see that the coloration of the AgI-AgPO₃-WO₃ glasses changes drastically from pale-yellow to orange and finally to black with increasing WO₃ concentration. According to the abovementioned synthesis procedure, it was not possible to obtain homogeneous bulk vitreous samples for concentration of WO₃ above 25 mol%. The glassy nature of the prepared samples was confirmed by X-ray diffraction (XRD) as shown in Fig. 2a for the 45AgI-40AgPO₃-15WO₃ glass composition. The XRD patterns recorded on the other glass compositions are presented in the ESI (Fig. S1 to S5†). Their respective glass transition temperature (T_g) was determined by DSC analysis. A typical DSC thermogram, recorded from the 45AgI-40AgPO₃-15WO₃ glass, is presented in Fig. 2b. The glass transition temperature for the 15 mol% WO₃ glass composition was determined at $T_g = 204$ $^{\circ}\text{C}$ (onset temperature).

The preparation method strongly influences the thermal properties of AgPO₃ because of residual water affecting the AgPO₃ glass.⁴¹ Depending on the method used, the glass transition temperature T_g of AgPO₃ may vary between 110 and 189 $^{\circ}\text{C}$, and the onset crystallization temperature T_x between 255 and 313 $^{\circ}\text{C}$. Therefore, in order to ensure reproducibility in

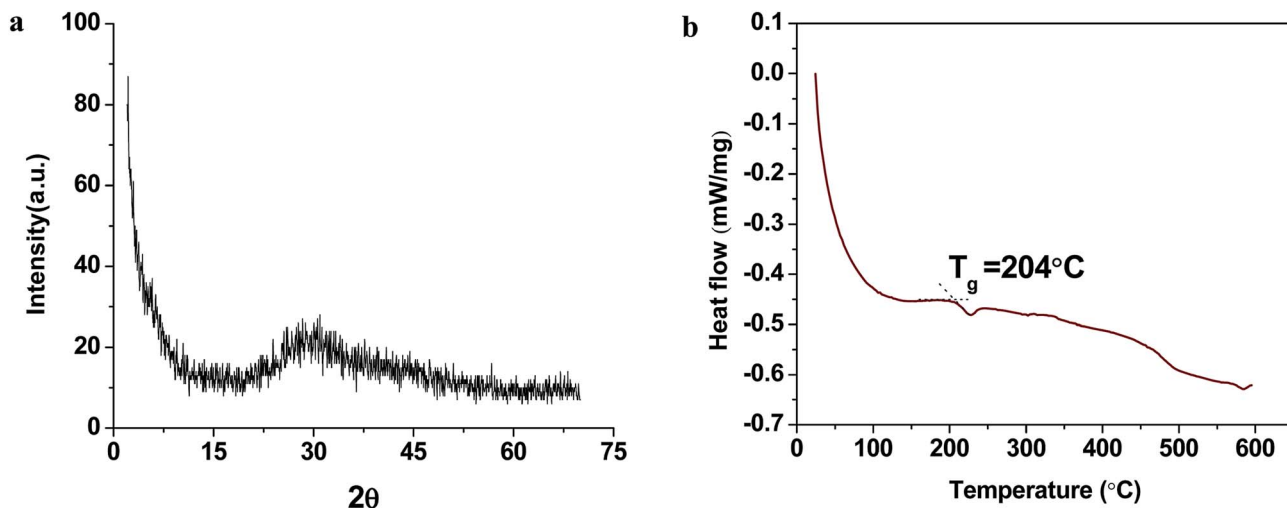


Fig. 2 XRD pattern of the 45AgI-40AgPO₃-15WO₃ glass (a) and DSC thermogram of the 45AgI-40AgPO₃-15WO₃ glass (b).

the preparation of AgI-AgPO₃-WO₃ glasses, each batch of AgPO₃ was first prepared following strictly similar conditions and then characterized by DSC analysis prior to any utilization as starting material. Through the method used in the present study, the characteristic temperatures of AgPO₃ were

determined at $T_g = 160 \pm 4$ °C and $T_x = 300 \pm 4$ °C. The DSC thermogram of the AgPO₃ glass is presented in the ESI (Fig. S6†). It is worth noting that no crystallization peaks were detected for the studied AgI-AgPO₃-WO₃ glasses under the conditions used for the DSC measurements (10 °C min⁻¹ up to 600 °C). Such absence of crystallization peaks on DSC curves has already been reported in AgI-AgPO₃ based glasses with AgI molar concentration above 20%.⁴² The addition of AgI to the AgPO₃ glass influences substantially its thermal properties of the glass, especially by decreasing its T_g as it has been demonstrated by Novita *et al.*⁴³ Originally, AgPO₃ has a stressed rigid glass network made of polymeric chains of PO₄ tetrahedral units.^{43,44} By adding ≥ 10 mol% of AgI to the AgPO₃ network, ring-like structures are formed, decreasing its connectivity and the glass transition temperature T_g .

On the other hand, as can be seen in Fig. 3, addition of WO₃ results in a continuous increase of the glass transition temperature T_g . Such behavior was expected due to the high melting temperature of WO₃ (1473 °C). Tungsten (W) in WO₃ has a high oxidation number (M^{z+} , $z = 6$). Consequently, the electrostatic field (z/a^2 , with a representing the ionic radius) of W^{6+} is high, which means that the interaction with the non-bridging oxygens forming P-O-M links is quite strong, strengthening the network cohesion, thus increasing the viscosity and the T_g of the glass. Similar effects are observed with the addition of WO₃ in other phosphate glasses belonging to the vitreous systems NaPO₃-WO₃, NaPO₃-Al₂O₃-WO₃ and K₂O-B₂O₃-P₂O₅-Nb₂O₅-WO₃.⁴⁵⁻⁴⁷ As shown in Fig. 3, the T_g of AgI-AgPO₃-WO₃ glasses can be adjusted continuously and reproducibly by varying the concentration of WO₃. In addition, the thermal expansion coefficient (TEC) determined from room temperature up to 100 °C on these glasses can be adjusted by varying the concentration of WO₃. Knowledge of glass thermal expansion coefficient is usually essential in optical fiber fabrication, particularly when core/cladding fibers have to be co-drawn from a same glass preform. The co-drawing of two glass materials of different compositions usually implies an

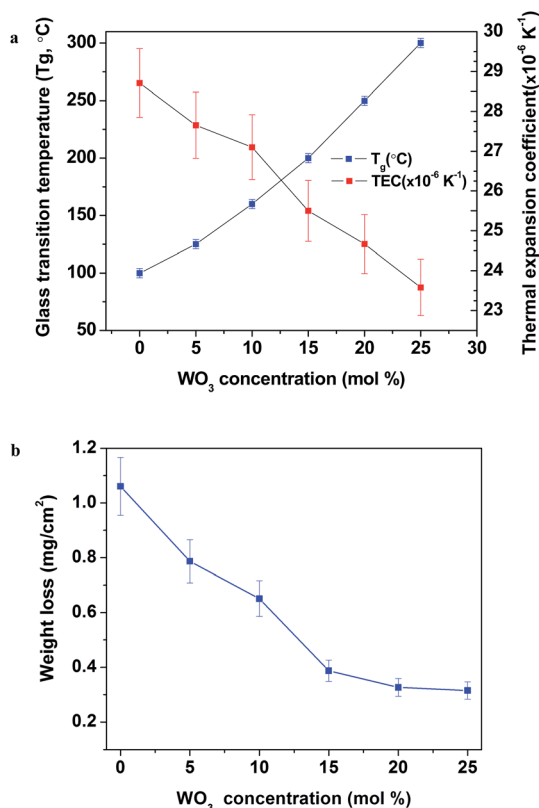


Fig. 3 Glass transition temperature (T_g) and thermal expansion of coefficient (TEC) of the 45AgI-(55 - x)AgPO₃-xWO₃ glasses as a function of molar concentration of WO₃ (a) and 60 °C/48 h water soak test on AgI-AgPO₃-WO₃ glass samples, as a function of WO₃ molar concentration (b).

Table 1 Elemental micro-analysis of 45AgI-(55 - x)AgPO₃-xWO₃ glasses, and weight percentages of every elements present in the glass compositions

x	wt% Ag		wt% I		wt% P		wt% W		wt% O	
	Th	Exp	Th	Exp	Th	Exp	Th	Exp	Th	Exp
0	51.7	57.9 ± 0.7	27.4	24.0 ± 0.5	8.2	6.6 ± 0.1	0.0	0.0	12.7	11.3 ± 0.3
5	48.7	53.6 ± 0.2	27.1	24.3 ± 0.1	7.3	6.3 ± 0.2	4.4	3.9 ± 0.4	12.5	11.4 ± 0.4
10	45.7	50.4 ± 0.2	26.8	24.7 ± 0.2	6.5	5.7 ± 0.1	8.6	7.9 ± 0.4	12.4	11.2 ± 0.4
15	42.6	47.7 ± 0.3	26.5	24.2 ± 0.2	5.8	5.2 ± 0.1	12.8	12.1 ± 0.4	12.3	10.9 ± 0.3
20	39.7	45.0 ± 1.0	26.3	22.7 ± 1.3	5.0	4.6 ± 0.1	16.9	15.8 ± 0.4	12.1	12.0 ± 1.0
25	36.9	41.7 ± 0.2	26.0	25.7 ± 0.2	4.2	3.9 ± 0.0	20.9	19.5 ± 0.3	12.0	11.2 ± 0.3

excellent matching of their thermal properties, including their softening temperature, viscosity vs. temperature, and TEC. One can clearly observe in Fig. 3 a linear decrease of the TEC of the AgI-AgPO₃-WO₃ glasses, from 29 to 24 × 10⁻⁶ K⁻¹, with increasing WO₃ concentration from 0 to 25 mol%, respectively. This agrees with the reticulation effect of WO₃ into the glass network. Furthermore, water soak tests were performed to

characterize the effect of WO₃ on the glass stability under wet conditions. To that end, the AgI-AgPO₃-WO₃ glass samples were soaked in 60 °C temperature deionized water for a period of 48 hours, and inspected for weight loss per surface area. As shown in Fig. 3, significant reduction of glass solubility into water occurred with increasing WO₃ concentration. As WO₃ is a Lewis acid, it interacts with the oxygen atoms into the

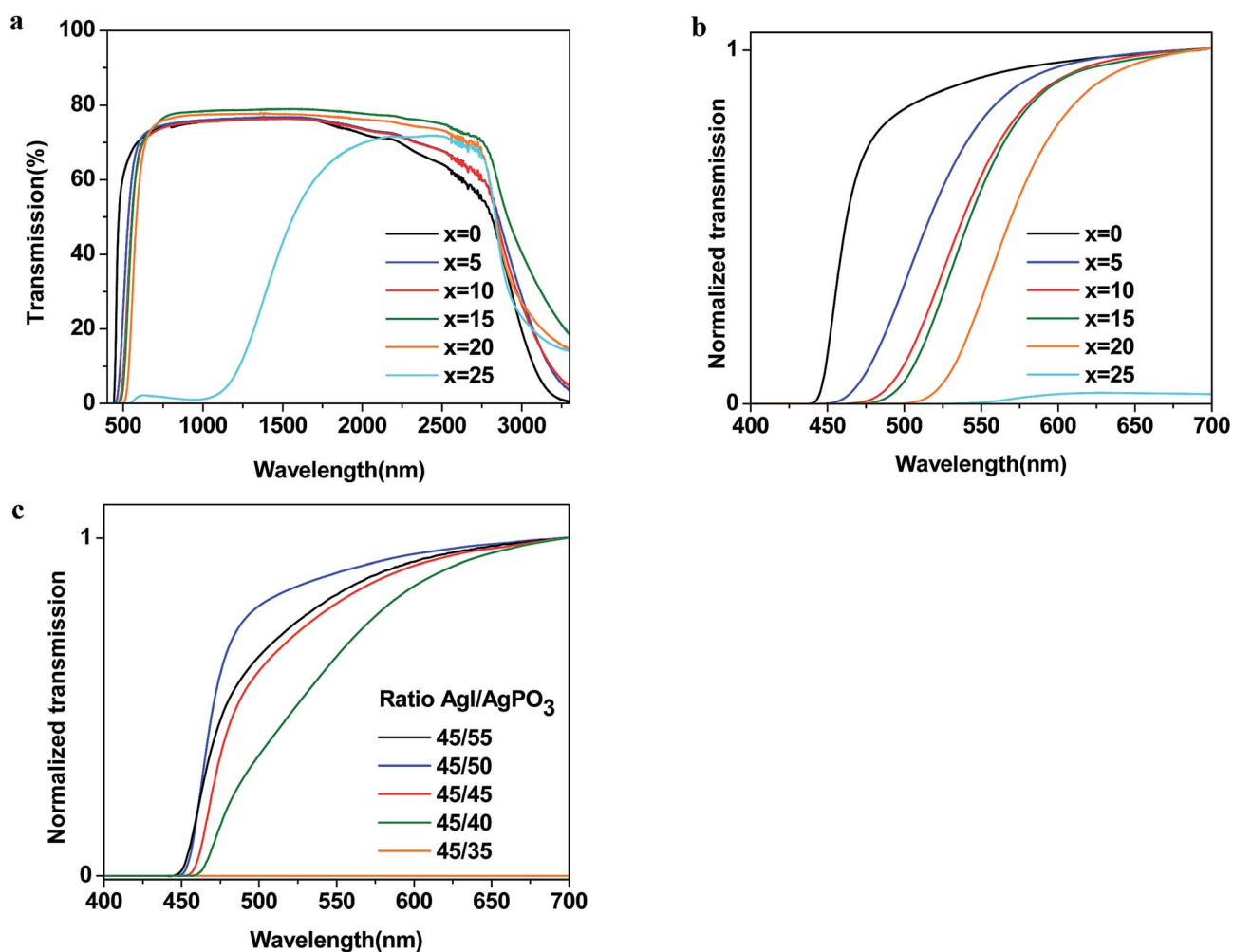


Fig. 4 Transmission spectra of 45AgI-(55 - x)AgPO₃-xWO₃ glasses as a function of WO₃ content (a), normalized visible transmission spectra (b) and normalized visible transmission spectra of pseudo-binary AgI-AgPO₃ glasses with the same ratios AgI/AgPO₃ than the (45AgI)-(55 - xAgPO₃)-(xWO₃) glasses (c). Samples thickness: 3 mm.

phosphate matrix and prevents hydrolysis reactions, thus improving the glass resistance to water in the environment.

Table 1 summarizes the experimental (Exp) and theoretical (Th) elemental compositions in wt% for each glass composition as a function of WO_3 content. For each glass composition, three samples have been investigated with eight quantitative measurements. The measurement error bars have been determined with a confidence level of 99%. As can be seen, the concentration of the elements for each material showed small sample-to-sample variations demonstrating that the above-mentioned synthesis method provides good reproducibility. Except for silver, all other elements showed some material loss during the synthesis. The major loss comes from iodide, because of its high vapor pressure, and phosphorus that can interact with environmental water to form phosphoric acid (H_3PO_4) which is volatile at high temperature. These could explain the higher experimental weight percentages obtained for silver.

3.2 Optical characterizations

The transmission spectra of the $\text{AgI-AgPO}_3\text{-WO}_3$ glasses are presented in Fig. 4a and b as a function of WO_3 content. One can observe that increasing the amount of WO_3 results in a concomitant shift of the glass optical band edge towards longer wavelengths. Moreover, one can also note in Fig. 4b that glasses with low concentrations of WO_3 are optically transparent in the visible range, with optical band edges near 500 nm wavelength corresponding to electronic transition energies of about 2.5 eV, except for the $45\text{AgI-}30\text{AgPO}_3\text{-}25\text{WO}_3$ sample which is inhomogeneous with practically no transmission in the visible spectrum. It is important to understand the effect of addition of WO_3 on the light transmission of AgI-AgPO_3 glasses, which are pale yellow solids (Fig. 1). At high temperature, tungsten can react with water or iodide to form different compounds which change the optical band edge and transmission spectrum. For instance, above $300\text{ }^\circ\text{C}$ and in presence of atmospheric moisture, we may observe the formation of ditungsten trioxide monohydrate ($2\text{WO}_3\text{-H}_2\text{O}$) which is an orange yellow colored solid.⁴⁸ Then, tungsten-iodide compounds may also be formed, like black tungsten

tetraiodide (WI_4), gray tungsten triiodide (WI_3) or brown-orange tungsten diiodide (WI_2).⁴⁹ Furthermore, in the absence of oxygen during the melting, the W^{6+} ions can be reduced into W^{5+} by the non-bridging oxygens of the phosphate matrix, or by hydrogen absorption under heat treatment in the presence of water vapor. In that case, the tungsten blue oxide (TBO) can form, where the blue color is due to W^{5+} ions as previously reported.^{50,51} Usually, for glasses prepared under normal conditions, *i.e.* neither oxidant nor reductive conditions, such reduction of W^{6+} to W^{5+} can be observed for relatively large concentration of tungsten oxide, typically above 15 mol%. Therefore, we can assume the presence of TBO, which could explain the observed greenish clouds inside the materials and opaque black solids at high concentration of WO_3 (*i.e.* $x \geq 25\%$). As mentioned previously, many different tungsten compounds can form in these glasses, but it is difficult to know which one is formed and is responsible for the resulting color of the glasses. Moreover, as WO_3 is substituted for AgPO_3 , according to the composition law used in this work, increasing

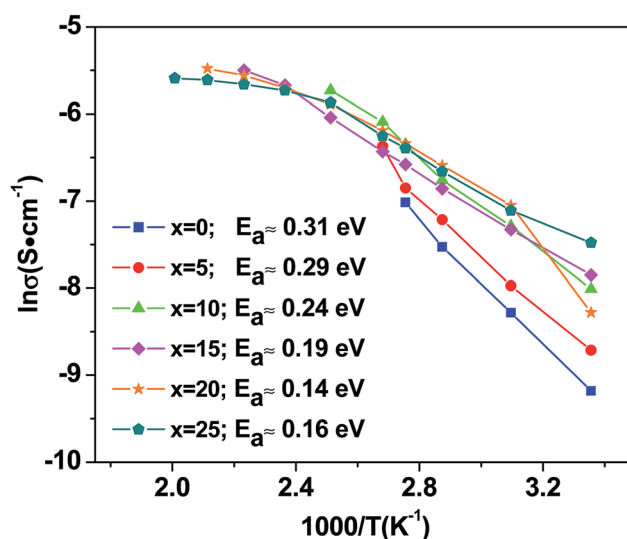


Fig. 6 Electrical conductivity of the $45\text{AgI-(}55-x\text{)AgPO}_3\text{-}x\text{WO}_3$ glasses at an AC frequency of 1 MHz, as function of temperature and glass composition. Applied voltage: 100 mV.

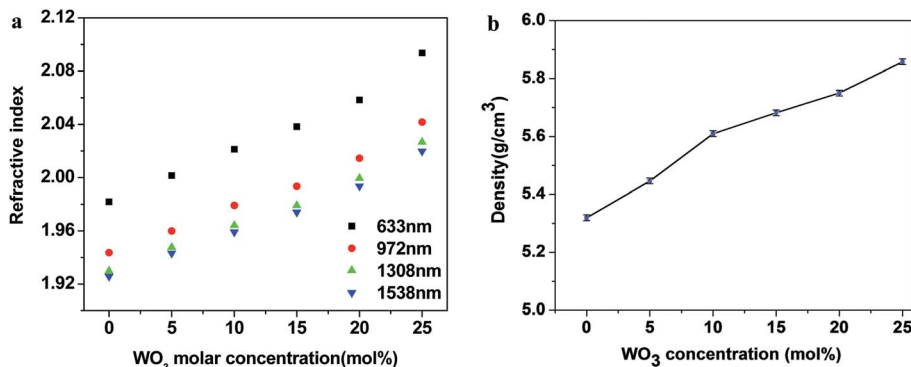


Fig. 5 Refractive index at 633, 972, 1308 and 1538 nm for $45\text{AgI-(}55-x\text{)AgPO}_3\text{-}x\text{WO}_3$ glasses as a function of WO_3 content, measured with an accuracy of ± 0.001 (a) and measured glass density as a function of WO_3 content (b).

the WO_3 content implies a decrease of AgPO_3 content, which may play a role in the glasses color change. Additional pseudo-binary AgI-AgPO_3 glass samples were thus prepared according to the same fabrication method by maintaining the same AgI/AgPO_3 molar ratios, *i.e.* $\text{AgI/AgPO}_3 = 45/55, 45/50, 45/45, 45/40, 45/35$ and $45/30$. First, homogeneous glass samples were obtained only from the ratios $\text{AgI/AgPO}_3 = 45/55, 45/50, 45/45, 45/40$, illustrating therefore the role played by WO_3 for the glass formation. Tungsten oxide WO_3 is considered as a glass intermediary and can act as a glass-former and/or glass-modifier depending on the glass network. Then, from the visible transmission spectra of the prepared AgI-AgPO_3 glasses presented in Fig. 4c, one can observe that the glass optical band edge shifts towards longer wavelengths when increasing the AgI/AgPO_3 ratio, or when decreasing the relative AgPO_3 content or increasing the relative iodine content. No significant photoconductive effects were measured when shining blue light on the glass samples.

The measured refractive index of the glass without WO_3 is on the order of 1.9. Such high value of refractive index can be

explained by the large content of highly polarizable I^- anions ($\alpha \text{ (cm}^3\text{)} = 7.1 \times 10^{-24}$).⁵² Progressive addition of WO_3 to the glass matrix resulted in a continuous increase of the glass refractive index, as shown in Fig. 5a, as well as an increase of the glass density, as shown in Fig. 5b. Therefore, the refractive index can be fine-tuned in the range from 1.9 to 2.1 with the addition of WO_3 to the glass, which opens many applications in fiber optics where adjustable numerical aperture may be highly desirable.

3.3 Bulk glasses electrical characterizations

Electrical conductivity measurements, under alternate current (AC) frequencies between 1 Hz and 1 MHz, have been carried out for the $\text{AgI-AgPO}_3\text{-WO}_3$ glasses as a function of temperature and WO_3 concentration, up to temperatures close to that of glass transition for each glass samples. The electrical conductivity of the glasses was calculated using:

$$\sigma = \frac{l}{ZS} \quad (1)$$

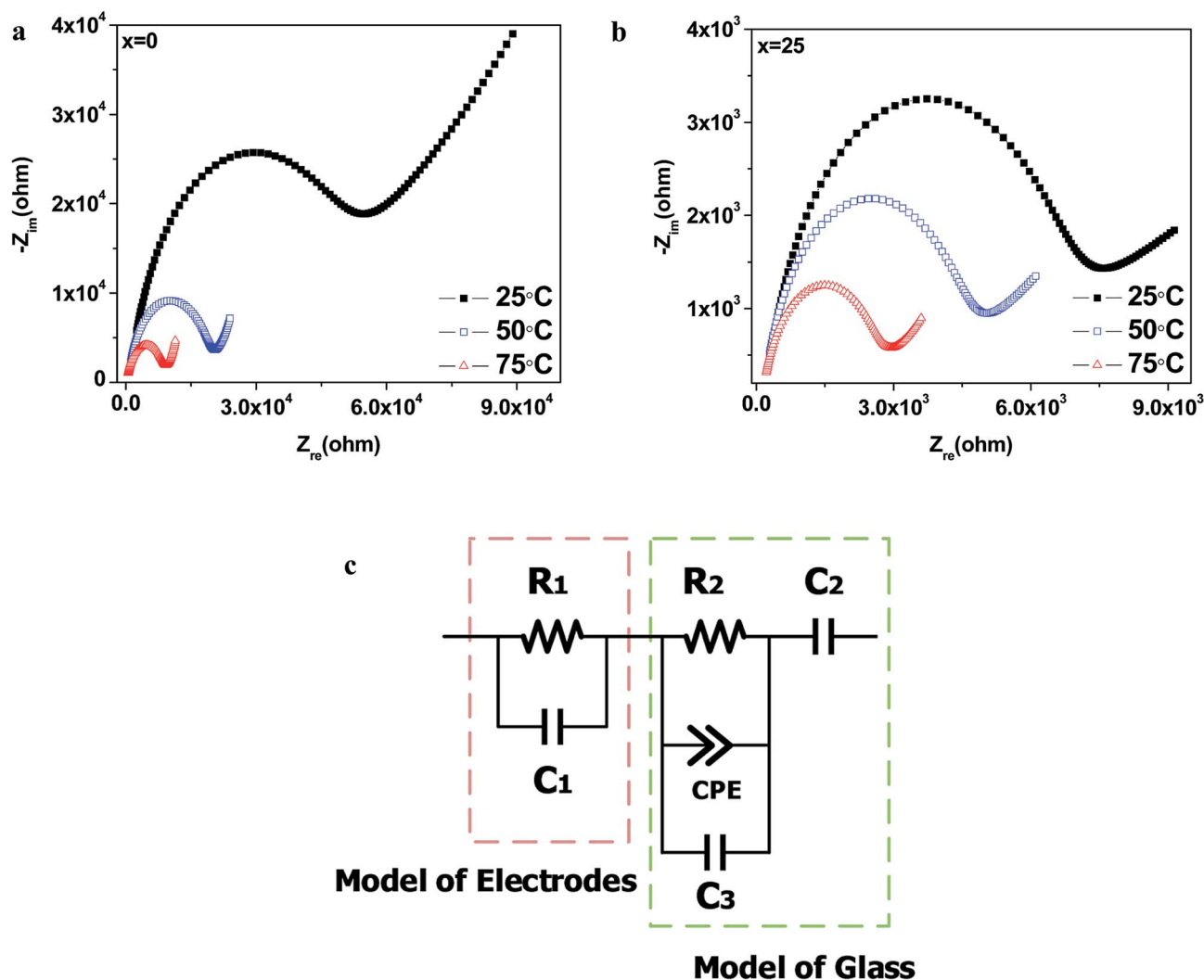


Fig. 7 Nyquist complex impedance spectra of the $45\text{AgI}-(55-x)\text{AgPO}_3-x\text{WO}_3$ glasses as a function of temperature for $x = 0$ (a) and $x = 25$ (b), and equivalent circuit consisting of electrode (R_1, C_1) and glass material contributions ($R_2, C_2, \text{CPE}, C_3$) (c). Applied voltage: 100 mV.

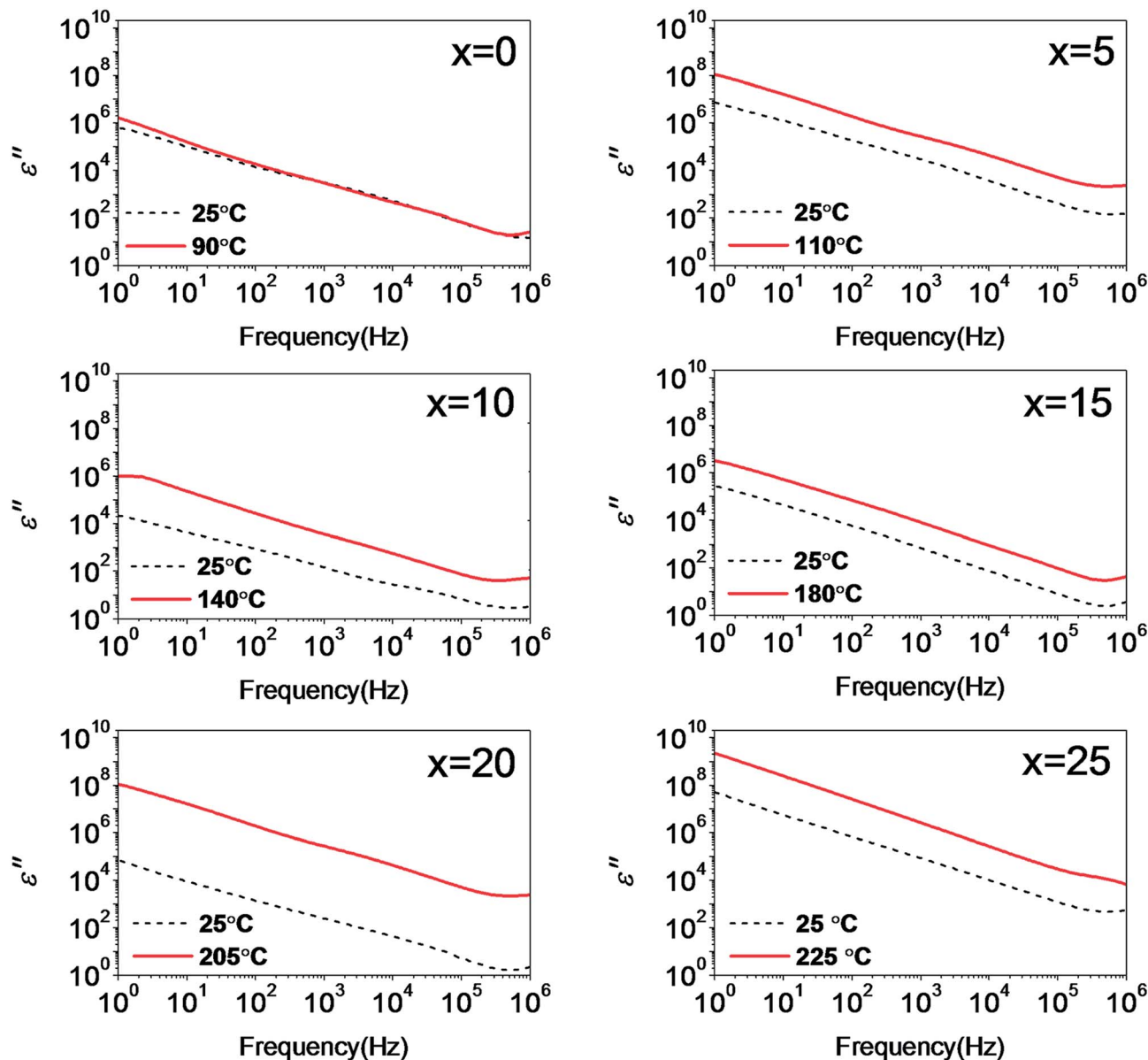


Fig. 8 Frequency–temperature dependent relative imaginary permittivity measurements of $45\text{AgI}-(55-x)\text{AgPO}_3-x\text{WO}_3$ glasses.

where σ is the conductivity, l the sample thickness, Z the impedance magnitude and S the surface area of the sample. Fig. 6 presents glass electrical conductivities at 1 MHz frequency as a function of temperature; it can be seen that the electrical conductivities increase with temperature for all glass compositions, commensurate with thermal activation energies ranging from 0.15 to 0.30 eV, wherein increased WO_3 concentration leads to higher AC conductivities and lower thermal activation energies. The appearance of a dual slope in the Arrhenius plot for WO_3 concentrations of $x \geq 20$ may be attributable to the presence of two different conductivity mechanisms in the glass within this temperature range, with thermal activation energies below 0.20 eV. Since the measured thermal activation energies were well below the ~ 2.5 eV electronic transition energies mentioned previously, and since the

glasses did not show significant photoconductive effects, it can be inferred that valence-to-conduction electronic transitions are not a dominant conductivity mechanism for these glasses, and that the dominant conductivity mechanism is ionic in nature.

The AC glass electrical conductivity at 1 MHz is on the order of 10^{-3} S cm^{-1} for all the studied compositions, in agreement with previously published studies on $45\text{AgI}-55\text{AgPO}_3$ glasses.^{53–55} As a first assumption, we propose that the increasing amount of WO_3 in the glass increases the formation of tungsten-iodide compounds, and consequently the silver ions are less attracted by the iodide anions which facilitates their mobility inside the glass network. Also, it has been demonstrated by Raman spectroscopy that structural abnormalities in $\text{AgI}-\text{AgPO}_3$ glasses could be the cause of variations as high as 35% of the ionic conductivity for the same molar

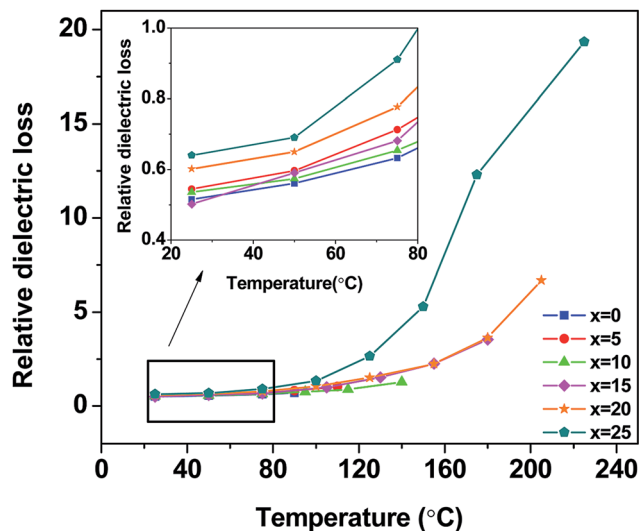


Fig. 9 Temperature dependent relative dielectric loss measurements of $45\text{AgI}-(55-x)\text{AgPO}_3-x\text{WO}_3$ glasses as a function of WO_3 concentration. The inset is a magnification of the relative dielectric loss between 20 and 80 °C.

concentration of AgI, and that water contamination could also produce variations in the electric conductivity.⁴³ The origin of the effect of WO_3 on the different glasses remains unclear, but the study shows that it can promote the electrical conductivity of the glass using the preparation method mentioned above.

We have also investigated the complex impedance of the glasses to characterize the materials under AC current. Fig. 7 shows two examples of Nyquist complex impedance spectra recorded at three different temperatures on samples $x = 0$ and 25 mol%. The Nyquist complex impedance spectra obtained for the other glass compositions are presented in the ESI (Fig. S7 to S10†). The measured Nyquist profiles are indicative of a resistance–capacitance parallel circuit behavior that comprises a phenomenological constant phase element (CPE). The CPE is a component that models impedance elements exhibiting distributed materials properties, and has been proposed to explain the behavior of ionic charge carriers in ionic conductors.⁵⁶ Equivalent circuits greatly aid in the process of fitting observed impedance data for elements with distributed properties. It has been shown in different studies that CPE behavior could represent the ions mobility in Li-ions borate conductive glasses^{57,58} and yttria stabilized zirconia (YSZ).⁵⁹ The CPE was an essential element that provided accurate modelization (within ~1% error) of the AgI–AgPO₃–WO₃ glass complex impedance of Fig. 7, for all range of compositions studied. The equivalent circuit that represents the conductivity of the glasses is schematized in Fig. 7c. This simple electrical model could be applied for all glass compositions investigated in the present study. The model assigns resistances and capacitances related to the electrodes (R_1 , C_1) and to the glass (CPE– C_2 – C_3 – R_2). Toward high frequencies, the glass-related capacitances (CPE– C_2 – C_3) are less dominant and the contribution of the electrodes is negligible, which mainly left the effect of the

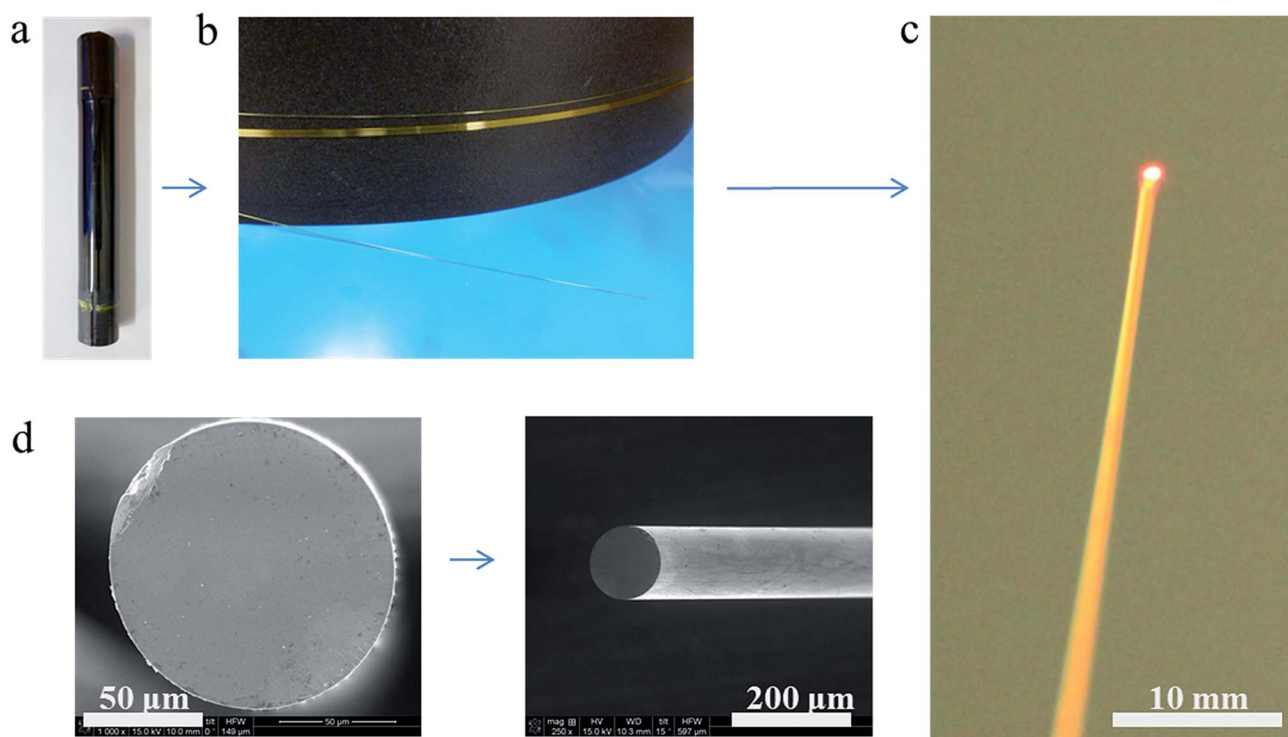


Fig. 10 Photograph of the $45\text{AgI}-40\text{AgPO}_3-15\text{WO}_3$ polished glass preform (a), photograph of the drawn optical fiber of (125 ± 5) μm diameter with acrylate polymer coating (b), photograph of the optical fiber without acrylate polymer coating showing the efficient transmission of light; scale bar: = 10 mm (c), and SEM images of the fiber without acrylate polymer coating; scale bar: 50 μm and 200 μm , respectively (d).

Table 2 Electrical conductivity of the 45AgI–40AgPO₃–15WO₃ glass fibers, as a function of the surface/volume ratio. Applied voltage: 100 mV; frequency: 1 MHz, accuracy: 0.1%

Sample diameter (±5 μm)	Surface/volume ratio	Conductivity (S cm ⁻¹)
125 (fiber)	320	0.428
250 (fiber)	120	0.140
1000 (bulk)	7.50	0.0004

conduction resistance of the glass (R_2). At low frequency, the response due to the electrodes becomes more prominent.

We have also performed frequency dependent relative imaginary permittivity (ϵ'' , also called dielectric loss factor) measurements between 1 Hz and 1 MHz. When an electric field is applied to a dielectric material, the charges become polarized to compensate for the electric field. Four dielectric polarization mechanisms may contribute to the dielectric loss factor ϵ'' of the material: ionic, dipolar, atomic and electronic polarizations. At low frequency (*i.e.* $<10^9$ Hz), the ionic polarization is very strong,

and the ϵ'' is inversely proportional to frequency and corresponds to $1/f$ of the slope which indicates that ϵ'' may be dominated by the influence of ionic conduction. Consequently, the ϵ'' slope can provide information about the electrical conductivity mechanism in the measured frequency range. Fig. 8 shows ϵ'' curves typical of $1/f$ behavior within the range of AC frequencies from 1 Hz to 1 MHz, with no other significant polarization mechanisms, for all compositions, and at room temperature and near T_g . Again, these results are indicative that the electrical conductivity of these glasses is predominantly ionic in nature.

The relative dielectric loss, which is the ratio of the relative imaginary permittivity (ϵ'') to the relative real permittivity (ϵ'), noted as $D_L = \epsilon''/\epsilon'$, has also been investigated as a function of temperature. ϵ'' and ϵ' represent the material capacity to dissipate electric energy and to store electric energy, respectively. Following the Debye theory for dielectric materials,^{60–62} ϵ'' takes into account electrical loss and can be expressed by the following equation:

$$\epsilon'' \approx \frac{\sigma(T)}{\epsilon_0 \omega} \quad (2)$$

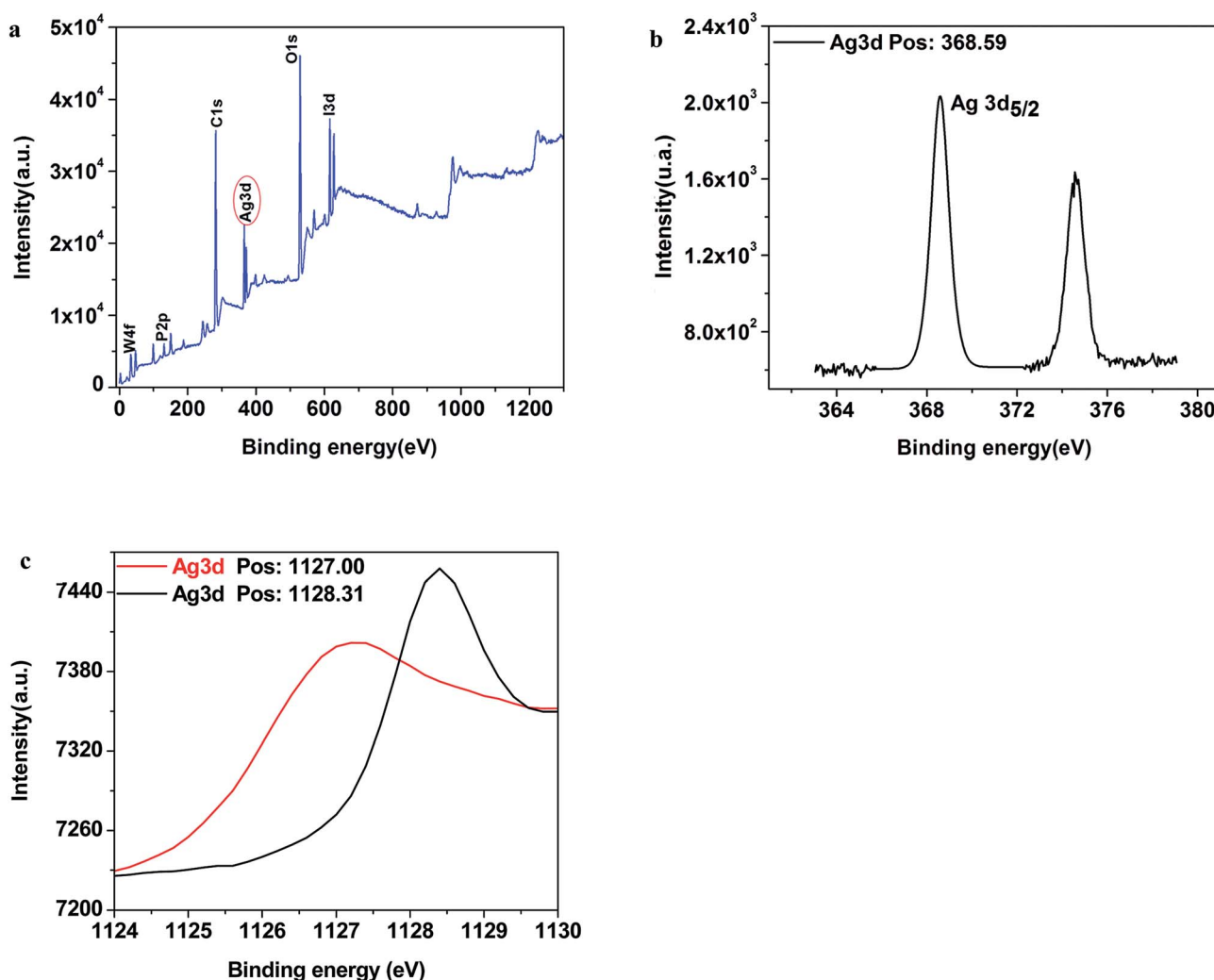


Fig. 11 XPS spectrum (a), high resolution Ag spectrum (b) and Ag-Auger $M_4N_{45}N_{45}$ spectra (c) for the 125 μm fiber.

where $\sigma(T)$ is the conductivity as a function of the temperature, ϵ_0 the vacuum permittivity and ω the angular frequency. From the results of Fig. 8 and 9, increasing temperature results in an increase of material electrical conductivity and relative dielectric loss. The increase of dielectric loss with temperature may be attributable to phonon-mediated carrier scattering in the glass, and to the generation of heat (*i.e.* friction) inside the glass. Furthermore, in Fig. 9, higher dielectric losses are observed for glasses containing larger concentration of WO_3 (*i.e.* $x = 20$ – 25 mol%), which could be attributed to the higher glass density.

3.4 Optical fibers characterizations

The 45AgI–40AgPO₃–15WO₃ vitreous composition was selected for optical fiber drawing as the best compromise among the studied glasses in terms of good thermal properties for fiber drawing (large difference between onset of crystallization and glass transition temperatures), high optical transmission in visible and short-infrared wavelengths, and high electrical conductivity. First, this glass composition exhibits thermal stability with no apparent crystallization which is an important property for good drawing capability of the glass into a fiber. Second, the transmission window covered by the glass is in the range between 450 and 2800 nm. The glasses showing the best transmission in visible light refer to $x = 0$ and 5 mol% WO_3 concentrations, but these compositions are not sufficiently stable in normal environmental humidity and thus cannot be used conveniently for fiber optics application. Moreover, the compositions with $x = 20$ and 25 mol% show volume inhomogeneities attributable to the reduction of the W^{6+} , which can strongly degrade optical transmission. The compositions $x = 10$ and 15 mol% provide high optical transmission between 500 and 2800 nm, and good chemical resistance against water. Also, the electrical conductivity of this glass is one of the best among those measured in this study. The 45AgI–40AgPO₃–15WO₃ glass composition provided the best set of attributes for fabricating high-transparency, high-conductivity, and environmentally stable optical fibers.

The 45AgI–40AgPO₃–15WO₃ glass preforms were drawn to multi-mode fibers, with a diameter of (125 ± 5) μm , using a standard fiber drawing tower set at a furnace temperature of 300 °C. The optical transparency of the glass fibers was lowest in the 700–1000 nm wavelength region, with a minimum propagation loss of about 2 dB m^{-1} in the short-infrared wavelength range from 800 to 950 nm. Following the fiber drawing, Scanning Electron Microscope (SEM) imaging was performed on the fibers (Fig. 10d) to confirm that the implemented conditions permitted good control and reproducibility of the fiber fabrication process. The quality control related to the absence of defects like crystallized particles or bubbles, and the absence of significant diameter variations over the whole fiber length was evidenced. The glasses of composition 45AgI–40AgPO₃–15WO₃ were easily drawn into fibers without apparent crystallization in the volume or at the surface of the glass. Furthermore, the fibers exhibited good mechanical strength even without the polymer coating, which made them very easy to manipulate. Interestingly, the comparison of the electrical conductivity of these

fibers with the bulk glass showed that drawing the glass led to an increase of its conductivity. During fiber drawing, the surface-to-volume ratio (S/V) of the glass increases, which means that surface conductivity may contribute to the overall electrical conductivity of the glass fiber. To explore this phenomenon further, we have fabricated fibers with different diameters to obtain different S/V ratios, and compared their electric conductivity with that of the bulk. As can be seen in Table 2, as the S/V ratio increased, the conductivity increased by three orders of magnitude, thus providing a wide range of electrical tunability for the fibers.

In order to verify that the observed S/V conductivity increase did not originate from any formation of metallic silver or silver oxide during the fiber drawing, XPS analyses have been performed on the 45AgI–40AgPO₃–15WO₃ glass bulk and fibers (of 125 and 250 μm diameter). The glass bulk was set on a stainless steel sample holder and the fibers were cut into small pieces to be placed in a copper sample holder. The fibers have been analyzed along the cylindrical surface. Fig. 11 presents the XPS spectra (Fig. 11a), the high resolution spectrum (Fig. 11b) and the Ag-Auger $\text{M}_4\text{N}_{45}\text{N}_{45}$ spectra (Fig. 11c) for the 125 μm fiber. The XPS spectra recorded on the bulk, the 250 μm fiber, and the Ag standard are presented in the ESI (Fig. S11 to S17†). The C1s spectrum was recorded in order to correct the measured binding energies (BE). Indeed, the utilization of neutralizing canon tends to over compensate the charges that are created on the samples surface under photon bombardment. An internal standard or an element with known BE in the sample can be used for the correction. In the absence of a reliable internal reference, it is usually recommended to use the contamination or aliphatic carbon which is imposed with BE of 285 eV. This correction was applied on all the spectra of the same sample recorded under the same conditions of neutralization. The decompositions of the carbon C1s highlight, beside the aliphatic atoms, two types of carbon–oxygen bonding: C–O and O=C–O. High-resolution spectra of Ag provide, after correction, a BE equal to 368.5–368.6 eV for all the samples, which correspond to silver oxide (Ag_2O).^{63,64} This is slightly higher than what is expected with metallic silver, *i.e.* 368.25 eV. The absence of silver in its metallic form is confirmed by considering the Ag-Auger $\text{M}_4\text{N}_{45}\text{N}_{45}$ spectra. Although the Auger spectrum was not recorded on the glass bulk, the large intensity achieved in the XPS spectrum allowed the measurement of peak energy at 1128 eV with reasonable precision. Such value, coupled with the $\text{Ag}3\text{d}_{5/2}$ BE of 365.4 eV, allows us to calculate the modified Auger parameter, giving a value of 724 eV, which is attributed to the presence of Ag_2O while a value of 726 eV is expected for metallic silver Ag^0 .^{63,64} In the case of the 125 and 250 μm fibers, Auger spectra were recorded (Fig. 11c and S15†), leading to Auger parameters of 724.1 eV and 724.7 eV, respectively. Again the measured values are still far from the expected value for Ag^0 . Immediately after the sample analyses, the Ag^0 standard was analyzed after argon ion etching to produce a clean metal surface. The $\text{Ag}3\text{d}_{5/2}$ BE corresponds to 368.23 eV, as expected. The modified Auger parameter obtained was 726.3 eV, in perfect agreement with published data.^{63,64} This last result

confirms thus the previous ones: the $\text{Ag}3d_{5/2}$ binding energy on the glass bulk and the fibers is definitely slightly higher than that of Ag^0 and not due to a calibration error of the instrument. According to these analyses, there is no evidence of metallic silver Ag^0 in the glass bulk neither in the fibers. Very low relative atomic content of 5%, 1.5% and 3.5% (with an accuracy of 10%) were indeed measured for these silver species at the surface of the bulk, the 125 and the 250 μm fibers, respectively. Interestingly, there is no increase and/or tendency in the concentration of these species from the bulk to the fiber, which let us think that the stretching of the glass into a fiber could not affect significantly their formation. We conclude that such low concentrations of silver oxide measured in the samples cannot explain, alone, the large conductivity increase observed in the fibers. Indeed, previous investigations carried out on Ag_2O -based glasses have shown that high molar concentrations of Ag_2O are required to significantly impact on the glass conductivity.^{65–69} At these low concentrations, it is probable that silver oxide Ag_2O is simply formed upon exposure with the ambient air during the formation of the glass and the stretching of the fibers. Furthermore, the UV-Vis spectra for the bulk glasses do not show any absorption band that could result from the presence of silver nanoparticles or clusters plasmon.⁷⁰

4. Conclusion

In this study, we report to our knowledge the first optically-transparent and electrically-conductive optical glass fiber within the system $\text{AgI-AgPO}_3\text{-WO}_3$. The addition of tungsten oxide (WO_3) into the phosphate glasses allowed the adjustment of the glass transition temperature, thermal expansion coefficient, refractive index, optical band edge, and electrical conductivity, which are all very important parameters in view of drawing glass fibers with a desired set of electro-optical properties. Furthermore, the addition of WO_3 can improve considerably glass stability against water and humidity in the environment. $\text{AgI-AgPO}_3\text{-WO}_3$ glass fibers with 15 mol% WO_3 showed 2 dB m^{-1} optical propagation loss from 800 to 950 nm wavelength range, and $10^{-3} \text{ S cm}^{-1}$ electrical conductivity at 1 MHz AC frequency. Complex impedance spectra and thermal activation energies ranging from 0.15 eV to 0.30 eV are indicative of a dominant conductivity mechanism being ionic in nature within the range of AC frequencies from 1 Hz to 1 MHz. Fibers exhibited higher electrical conductivities than the bulk glasses. The XPS analyses have confirmed that the conductivity increase did not originate from the formation of metallic silver or silver oxide, since the former has not been detected while the latter was found in too low concentration to have any influence on the conductivity. This study let us think that the increase of conductivity in fiber form is predominantly a surface phenomenon. Given these properties, glasses in the $\text{AgI-AgPO}_3\text{-WO}_3$ system can be used for fibers that require good electrical conductivity, good optical transparency, as well as good environmental stability.

Acknowledgements

This research was supported by the Canadian Excellence Research Chair program (CERC) in Photonics Innovations. The authors are also grateful to the Natural Sciences and Engineering Research Council of Canada (NSERC), the Fonds de Recherche Québécois sur la Nature et les Technologies (FRQNT) and the Canadian Foundation for Innovation (CFI) for the financial support. The authors would like to thank Frédéric Lessard and Michel Jean for their technical support.

References

- 1 F. Sorin, A. F. Abouraddy, N. Orf, O. Shapira, J. Viens, J. Arnold, J. D. Joannopoulos and Y. Fink, *Adv. Mater.*, 2007, **19**, 3872–3877.
- 2 G. Tao, A. M. Stolyarov and A. F. Abouraddy, *Int. J. Appl. Glass Sci.*, 2012, **3**, 349–368.
- 3 S. Gorgutsa, V. Bélanger-Garnier, B. Ung, J. Viens, B. Gosselin, S. LaRoche and Y. Messaddeq, *Sensors*, 2014, **14**, 19260–19274.
- 4 H. S. Liu, T. S. Chin and S. W. Yung, *Mater. Chem. Phys.*, 1997, **50**, 1–10.
- 5 A. El Hadrami, H. Aouad, M. Mesnaoui, A. Maazaz and J.-J. Videau, *Mater. Lett.*, 2002, **57**, 894–898.
- 6 A. El Hadrami, M. Mesnaoui, M. Maazaz and J. J. Videau, *Phys. Chem. News*, 2007, 138–142.
- 7 L. Koudelka, J. Pospíšil, P. Mošner, L. Montagne and L. Delevoe, *J. Non-Cryst. Solids*, 2008, **354**, 129–133.
- 8 T. Fujiwara, D. Wong, Y. Zhao, S. Fleming, S. Poole and M. Sceats, *Electron. Lett.*, 1995, **31**, 573–575.
- 9 A. F. El-Sherif and T. A. King, *Opt. Commun.*, 2003, **218**, 337–344.
- 10 Y. LeChasseur, S. Dufour, G. Lavertu, C. Bories, M. Deschênes, R. Vallée and Y. De Koninck, *Nat. Methods*, 2011, **8**, 319–325.
- 11 A. Lymberis and S. Olsson, *Telemed. J. e-Health*, 2003, **9**, 379–386.
- 12 L. Van Langenhove, *Smart textiles for medicine and healthcare: materials, systems and applications*, Elsevier, 2007.
- 13 D. Kunze, *Solid State Batteries and Devices*, 1973, vol. 405.
- 14 G. Robert, J. P. Malugani and A. Saida, *Solid State Ionics*, 1981, **3–4**, 311–315.
- 15 T. Minami, *J. Non-Cryst. Solids*, 1983, **56**, 15–26.
- 16 S. W. Martin, *J. Am. Ceram. Soc.*, 1991, **74**, 1767–1784.
- 17 P. Boolchand and W. J. Bresser, *Nature*, 2001, **410**, 1070–1073.
- 18 H. Mehrer, *Diffusion in solids: fundamentals, methods, materials, diffusion-controlled processes*, Springer, 2007.
- 19 M. Tatsumisago, T. Saito and T. Minami, *Phys. Chem. Glasses: Eur. J. Glass Sci. Technol., Part B*, 2001, **42**, 215–219.
- 20 M. Tatsumisago, K. Okuda, N. Itakura and M. Tsutomu, *Solid State Ionics*, 1999, **121**, 193–200.
- 21 M. Tatsumisago, Y. Shinkuma and T. Minami, *Nature*, 1991, **354**, 217–218.
- 22 T. Saito, M. Tatsumisago, N. Torata and T. Minami, *Solid State Ionics*, 1995, **79**, 279–283.

- 23 M. Rie, Y. Takayuki, Y. Teppei, Y. Miho, I. Ryuichi, K. Hiroshi, K. Kenichi and T. Masaki, *Nat. Mater.*, 2009, **8**, 476–480.
- 24 B. Roling, M. D. Ingram, M. Lange and K. Funke, *Phys. Rev. B: Condens. Matter Mater. Phys.*, 1997, **56**, 13619.
- 25 M. Mangion and G. P. Johari, *Phys. Rev. B: Condens. Matter Mater. Phys.*, 1987, **36**, 8845.
- 26 G. Licheri, A. Musinu, G. Paschina, G. Piccaluga, G. Pinna and A. Magistris, *J. Chem. Phys.*, 1986, **85**, 500–506.
- 27 T. Minami, H. Nambu and M. Tanaka, *J. Am. Ceram. Soc.*, 1977, **60**, 467–469.
- 28 T. Minami, *J. Non-Cryst. Solids*, 1985, **73**, 273–284.
- 29 J.-P. Malugani and R. Mercier, *Solid State Ionics*, 1984, **13**, 293–299.
- 30 M. Tachez, R. Mercier, J. P. Malugani and A. J. Dianoux, *Solid State Ionics*, 1986, **20**, 93–98.
- 31 A. Musinu, G. Paschina, G. Piccaluga and G. Pinna, *Solid State Ionics*, 1989, **34**, 187–193.
- 32 K. J. Rao and C. N. R. Rao, *Mater. Res. Bull.*, 1982, **17**, 1337–1340.
- 33 M. D. Ingram, M. A. Mackenzie, W. Müller and M. Torge, *Solid State Ionics*, 1988, **28**, 677–680.
- 34 J. Bruce, A. M. D. Ingram, M. A. MacKenzie and R. Syed, *Solid State Ionics*, 1986, **18**, 410–414.
- 35 A. Chandra, A. Bhatt and A. Chandra, *J. Mater. Sci. Technol.*, 2013, **29**, 193–208.
- 36 M. D. Ingram, C. T. Moynihan and A. V. Lesikar, *J. Non-Cryst. Solids*, 1980, **38**, 371–376.
- 37 J. D. Wicks, L. Börjesson, G. Bushnell-Wye, W. S. Howells and R. L. McGreevy, *Phys. Rev. Lett.*, 1995, **74**, 726.
- 38 J. Swenson and L. Börjesson, *Phys. Rev. Lett.*, 1996, **77**, 3569–3572.
- 39 C. R. Gautam, D. Kumar and O. Parkash, *Bull. Mater. Sci.*, 2011, **34**, 1393–1399.
- 40 S. W. Anwane, *Adv. Mater. Lett.*, 2013, **4**, 300–309.
- 41 P. Mustarelli, C. Tomasi, A. Magistris and S. Scotti, *J. Non-Cryst. Solids*, 1993, **163**, 97–103.
- 42 F. Grosclaude, J. P. Malugani, C. Rousselot, R. Mercier and M. Tachez, *J. Phys.*, 1992, **2**, C2–C215.
- 43 D. I. Novita, P. Boolchand, M. Malki and M. Micoulaut, *Phys. Rev. Lett.*, 2007, **98**, 195501.
- 44 R. K. Brow, *J. Non-Cryst. Solids*, 2000, **263**, 1–28.
- 45 C. C. de Araujo, W. Strojek, L. Zhang, H. Eckert, G. Poirier, S. J. L. Ribeiro and Y. Messaddeq, *J. Mater. Chem.*, 2006, **16**, 3277–3284.
- 46 L. Montagne, G. Palavit, G. Mairesse, M. Draoui, K. Aomari and M. S. Idrissi, *Phys. Chem. Glasses*, 1997, **38**, 15–20.
- 47 L. Koudelka, J. Pospíšil, P. Mošner, L. Montagne and L. Delevoye, *J. Non-Cryst. Solids*, 2008, **354**, 129–133.
- 48 E. Lassner and W.-D. Schubert, *Tungsten: properties, chemistry, technology of the elements, alloys, and chemical compounds*, Springer, 1999.
- 49 J. D. Franolic, J. R. Long and R. H. Holm, *J. Am. Chem. Soc.*, 1995, **117**, 8139–8153.
- 50 G. Poirier, F. S. Ottoboni, F. Castro Cassanjes, Á. Remonte, Y. Messaddeq and S. J. L. Ribeiro, *J. Phys. Chem. B*, 2008, **112**, 4481–4487.
- 51 H. Tawarayama, F. Utsuno, H. Inoue, H. Hosono and H. Kawazoe, *Chem. Mater.*, 2006, **18**, 2810–2816.
- 52 L. Pauling, *General chemistry*, Courier Dover Publications, 2012.
- 53 M. Le Stanguennec and S. R. Elliott, *Solid State Ionics*, 1994, **73**, 199–208.
- 54 D. L. Sidebottom, *Phys. Rev. B: Condens. Matter Mater. Phys.*, 2000, **61**, 14507–14516.
- 55 M. Micoulaut, M. Malki, D. I. Novita and P. Boolchand, *Phys. Rev. B: Condens. Matter Mater. Phys.*, 2009, **80**, 184205.
- 56 J. R. Macdonald and E. Barsoukov, *Impedance Spectroscopy Theory, Experiment and Applications*, 2005, vol. 1, p. 8.
- 57 M. R. S. Abouzari, F. Berkemeier, G. Schmitz and D. Wilmer, *Solid State Ionics*, 2009, **180**, 922–927.
- 58 F. Berkemeier, M. R. S. Abouzari and G. Schmitz, *Phys. Rev. B: Condens. Matter Mater. Phys.*, 2007, **76**, 024205.
- 59 I. Kosacki, C. M. Rouleau, P. F. Becher, J. Bentley and D. H. Lowndes, *Solid State Ionics*, 2005, **176**, 1319–1326.
- 60 P. B. Ishai, M. S. Talary, A. Caduff, E. Levy and Y. Feldman, *Meas. Sci. Technol.*, 2013, **24**, 102001.
- 61 W.-l. Song, M.-s. Cao, Z.-l. Hou, J. Yuan and X.-y. Fang, *Scr. Mater.*, 2009, **61**, 201–204.
- 62 F. Henn, G. Garcia-Belmonte, J. Bisquert, S. Devautour-Vinot and J. C. Giuntini, *J. Non-Cryst. Solids*, 2008, **354**, 3443–3450.
- 63 J. F. Moulder, *et al.*, *Handbook of X-ray photoelectron spectroscopy*, Perkin-Elmer Corp, 1992.
- 64 S. W. Gaarenstroom and N. Winograd, *J. Chem. Phys.*, 1977, **67**, 3500.
- 65 N. Gupta and A. Dalvi, *Ionics*, 2011, **17**, 315–322.
- 66 K. Sklepić, M. Vorokhta, P. Mošner, L. Koudelka and A. Mogaš-Milanković, *J. Phys. Chem. B*, 2014, **118**, 12050–12058.
- 67 P. Sharma, D. K. Kanchan, N. Gondaliya, M. Pant and M. S. Jayswal, *New J. Glass Ceram.*, 2011, **1**, 125.
- 68 V. C. V. Gowda and R. V. Anavekar, *J. Mater. Sci.*, 2007, **42**, 3816–3824.
- 69 M. Tatsumisago, T. Saito and T. Minami, *Chem. Lett.*, 2001, 790–791.
- 70 M. Rycenga, C. M. Cobley, J. Zeng, W. Li, C. H. Moran, Q. Zhang, D. Qin and Y. Xia, *Chem. Rev.*, 2011, **111**, 3669–3712.